Three-Dimensional Structure Analyses of Cu Species Dispersed on TiO_2(110) Surfaces Studied by Polarization-Dependent Total-Reflection Fluorescence X-ray Absorption Fine Structure (PTRF-XAFS)

Yasuhiro Tanizawa,[†] Takafumi Shido,[†] Wang-Jae Chun,[‡] Kiyotaka Asakura,[‡] Masaharu Nomura,[§] and Yasuhiro Iwasawa*,[†]

Department of Chemistry, Graduate School of Science, The University of Tokyo, Hongo, Bunkyo-ku, Tokyo 113-0033, Japan, Catalysis Research Center (CRC), Hokkaido University, Kita 11-10, Kita-ku, Sapporo 060-0811, Japan, and Photon Factory, Institute of Materials Structure Science, High Energy Accelerator Research Organization (KEK−IMSS−PF), Oho 1-1, Tsukuba 305-0801, Japan

Received: May 14, 2003; In Final Form: September 2, 2003

Three-dimensional analysis of structures for dispersed Cu species on a TiO_2(110) surface has been performed by a polarization-dependent total-reflection fluorescence X-ray absorption fine structure (PTRF-XAFS) technique. The dispersed Cu species were prepared by a chemical reaction between $Cu(DPM)_2$ and a TiO_2(110) surface and reduced with H_2. The $Cu(DPM)_2$ dissociatively adsorbed on the 2-fold site of bridging oxygen atoms of the TiO_2(110) surface to form a $Cu(DPM)(O\text{-})_2$ species. Subsequent reduction of the Cu species with H_2 at 363 K produced Cu_3 trimers that were bound to the bridging oxygen atoms with the trimer plane inclined at about 30° from the TiO_2(110) normal. There were direct Cu−O bonds at the Cu_3 trimer/TiO_2(110) interface in addition to Cu−Cu bonds. Further reduction at 473 K produced three-dimensional prismatic small Cu_6 clusters by vertical growth in the [110] direction of the Cu fcc lattice. Orientations of the Cu_3 triangle and Cu_6 prism clusters may be regulated by the interaction between the Cu atoms and the bridging oxygen atoms on the anisotropic TiO_2(110) surface.

1. Introduction

Metal−metal oxide interfaces have drawn much attention for their wide applications to supported metal catalysts, photocatalysts, sensors, magnetic and electronic devices, and so on.[1−3] To understand the fundamental properties and interactions at metal−metal oxide interfaces, it is important to determine the interface structure and bonding feature in an atomic scale. Metals on the TiO_2(rutile)(110) surface have intensively been studied because of the high stability of the TiO_2(110) surface structure and its semiconductive property.[1] TiO_2 is also an important support material for metal to prepare dispersed metal catalysts. The TiO_2(110) (1 × 1) surface has an anisotropic structure as shown in Figure 1, where the protruding oxygen atoms called "bridging oxygen atoms" are running along the [001] direction.[1] There are 5-fold Ti and in-plane oxygen atoms in the troughs between the bridging oxygen rows. The structure has been confirmed by MEED, ICISS, ab initio calculation, XRD, STM, and AFM.[4−15] Metal particles have been deposited on the TiO_2(110) surface, and their morphology, growth mechanism, and electronic states have been investigated by STM, XRD, MEED, LEED, XPS, AES, UPS, ARPES, and so on. Diebold et al.[16] and Chen et al.[17] classified the structures of metal overlayers according to their reactivity. Early transition, alkaline, and alkaline earth metals such as V, Hf, Cr, Na, and Ca are relatively reactive to have a strong interaction with the support surface, where atomically dispersed or 2-dimensional overlayer

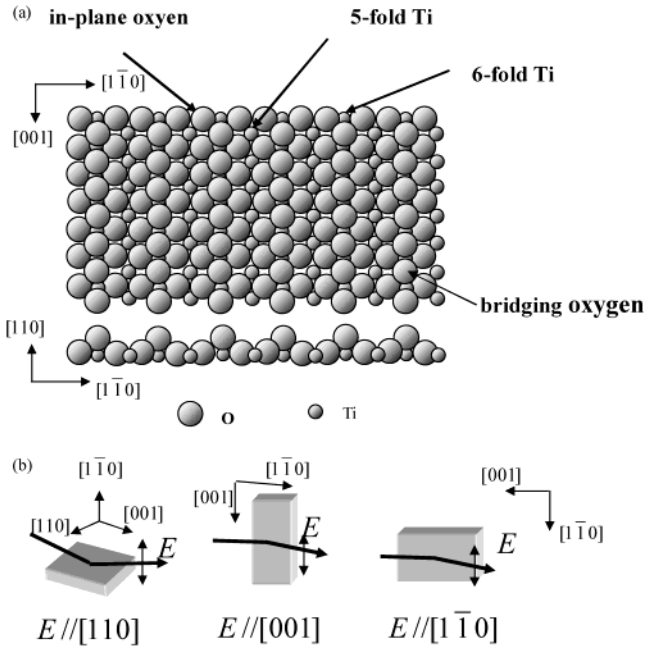

Figure 1. (a) Surface structure of TiO_2(110) and (b) orientations for the PTRF-XAFS measurements against the polarization electric vector.

growth is observed with a significant charge transfer from the TiO_2 substrate to the overlayer metals. Late transition metals such as Ni, Cu, Fe, Pt, Pd, Au, and Ag are less active which show three-dimensional particle growth (Volmer−Weber (VW) growth mode), although two-dimensional species and the Stransky−Krastanov (SK) growth mode have also been reported, depending on the preparation conditions.[17−22] Epitaxial growth

* To whom correspondence should be addressed. E-mail: iwasawa@chem.s.u-tokyo.ac.jp. Tel: 81-3-5841-4363. Fax: 81-3-5800-6892.
[†] The University of Tokyo.
[‡] Hokkaido University.
[§] Institute of Materials Structure Science.

10.1021/jp0306186 CCC: $25.00
Published on Web 11/01/2003

is frequently observed with fcc metals such as Ni, Cu, Pt, and Pd, where overlayer films grow in their (111) plane parallel to the TiO_2(110) surface and overlayer ($1\bar{2}1$) direction aligned to the substrate (001) direction.[18,20,23−29] Recently, STM and TEM studies indicated that fcc (110) planes grew parallel to the TiO_2(110) surface on some preparation conditions.[30,31] These studies provided information on the morphology, growth mechanism, electronic state, location, and registry of metal particles on the TiO_2(110) surface, but definite information about the chemical bonds of metal−metal oxides is still lacking, which allows us a deeper understanding of the chemical property of overlayer metals and the interaction of the overlayer metals with the substrate surface.

XAFS (X-ray absorption fine structure) is a technique to give the local structure around an X-ray absorbing atom. Up to now, the XAFS technique has widely been applied to examine the local structures of metal particles dispersed on powder metal oxides.[32,33] However, the metal−oxide interface structures derived from conventional XAFS are somewhat indecisive because of the powder samples which expose various crystal planes or have amorphous structures. Thus, single-crystal oxide surfaces are desirable to obtain the definite interface structure. In addition, polarization-dependent XAFS measurements are possible if single-crystal surfaces are used. The polarization dependence of XAFS can be given by eq 1[34]

$$\chi(k) = 3\sum_i \cos^2 \theta_i \, \chi_i(k) \qquad (1)$$

where $\chi(k)$,θ_i, and $\chi_i(k)$ are an overall XAFS oscillation, the angle between the *i*th bond direction and the electric vector of X-ray, and the partial XAFS oscillation accompanying the *i*th bond, respectively. When we use the polarized X-ray with its electric vector perpendicular to the surface of a single crystal, we can get information selectively toward the interface direction. On the other hand, when we use the polarized X-ray with its electric vector parallel to the surface, we will have the in-plane information selectively. To acquire the XAFS oscillations for the metal species deposited on the surface with the concentrations less than 10^{+14} atoms cm^{-2}, we have developed a polarization-dependent total reflection fluorescence XAFS technique (PTRF-XAFS).[34−38] Total reflection prevents the X-rays from penetrating into the bulk (the penetration depth equals a few nm) and tremendously increases the surface sensitivity of XAFS.[39] Moreover, the fluorescence detection mode enables us to obtain XAFS of dilute systems on the surface.[40] We have determined an anisotropic Mo−dimer structures supported on the TiO_2(110) surface and a Pt raft structure on Al_2O_3 (0001) by the PTRF-XAFS techniques.[36,41−44]

In this paper, we applied the technique to the local structure of Cu on TiO_2(110) prepared by using an organometallic compound. As mentioned above, Cu metals prepared by the metal vapor deposition technique grow in the VW growth-mode. Such 3-dimensional Cu metal particles are not always appropriate for the PTRF-XAFS investigation on the Cu−substrate interface structure because EXAFS oscillation perpendicular to the surface involves the Cu−Cu bond contribution in addition to the Cu−substrate one. Thus, we used a chemical attaching method to prepare well-dispersed Cu species on TiO_2(110) using a surface stoichiometric reaction between a Cu-complex precursor and the TiO_2 surface, followed by the reduction with H_2 under mild conditions.[45−48] $Cu(DPM)_2$ (DPM = dipivaloylmethanate, 2,2,6,6,-tetramethyl-3,5-heptadione) was employed as a precursor. The $Cu(DPM)_2$ reacts with the oxide surfaces to provide atomically dispersed species.[49,50] It is also reduced to a metallic state under mild conditions.[51] Thus, we can prepare Cu species with definite structures and chemical states, which interacted with the TiO_2 surface in a controllable manner.

The purpose of this paper is to study the interface structure around the Cu clusters derived from the $Cu(DPM)_2$ on a TiO_2-(110) surface by the PTRF-XAFS technique. In our previous report, we proposed a Cu_3 structure produced after reduction of H_2 at 363 K based on the curve fitting results.[52] The proposed Cu_3 structure had a strong Cu−O bonding at 0.171 nm, which is the shortest Cu−O bond distance ever reported, and a Cu−Ti bond was found at 0.248 nm in the [110] direction. We have carefully reanalyzed the EXAFS data and found a Cu_3 structure with a different orientation and interaction to the Al_2O_3 surface after the 363 K reduction. In this study, we have fully analyzed anisotropic Cu species after as-deposition of the $Cu(DPM)_2$ precursor, after reduction at 363 K, and after reduction at 473 K in three different directions on a TiO_2(110) surface by the PTRF-XAFS technique.

2. Experimental Section

2.1. Sample Preparation. An optically polished rutile TiO_2(110) single crystal with $20 \times 20 \times 1$ mm^3 (Earth Jewelry Co.) was pretreated at 673 K in air for 3 h to remove carbonaceous impurities and placed at a sample stage of a preparation chamber.[53] The treated TiO_2(110) surface showed a clear (1 × 1) LEED pattern. A precursor $Cu(DPM)_2$ was solved in diethyl ether under Ar atmosphere. The diethyl ether was dehydrated over Na wires and distillated before use as the solvent. The $Cu(DPM)_2$ solution was carefully added dropwise onto the TiO_2 substrate to prepare a homogeneously distributed Cu species under a flow of high purity Ar in the preparation chamber. After evacuation of the preparation chamber to 10^{-6} Pa, the sample was transferred to a high-precision 6-axis goniometer in the center of a measurement chamber without exposure to air. The base pressure of the measurement chamber was 5×10^{-8} Pa.

The loading of Cu on the TiO_2(110) surface was estimated to be about 0.3 ML by XPS equipped in the preparation chamber. The sample was treated in the measurement chamber with 1.33 kPa hydrogen at various temperatures (RT−473 K). XPS revealed that carbon was left and little Ti^{3+} was formed after the hydrogen treatment at 473 K.

2.2. XAFS Measurements. PTRF-XAFS measurements were performed at BL12C beam line of the Photon Factory in the Institute of Materials Structure Science, High Energy Accelerator Research Organization (PF−IMSS−KEK). The storage ring was operated at 2.5 GeV-300 mA. X-rays from the storage ring were monochromatized by a Si(111) double crystal monochromator and focused by a bent cylindrical mirror coated with Rh metal.[54] The critical energy of the mirror for total reflection conditions was set at 23 keV, which could efficiently remove the higher harmonics. Before an I_0 ionization chamber, the beam was collimated with a 0.2 mm pinhole slit in order not to illuminate the parts except the sample surface, which reduced the extra scatterings from the side of the sample or the sample holder. The incident X-ray intensity was monitored by a 5.5 cm long ionization chamber filled with N_2 gas. By using a goniometer, one can measure XAFS spectra in three different orientations of the sample as shown in Figure 1 and under their total reflection conditions without exposure to air. A typical total reflection angle was 5 mrad. The reflected and direct beams were monitored by an I ionization chamber filled with Ar that was set behind the measurement chamber. The fluorescent X-ray was detected by a NaI(Tl) scintillation counter. Usually, the

elastic scattering from the substrate still appears even in the total reflection conditions besides the fluorescence of the target element. In the case of Cu on TiO_2(110), Ti atoms in the substrate have a K-edge at 4964 eV, and they were excited by the direct and the scattered X-rays, giving intense Ti $K_{\alpha,\beta}$ fluorescence X-rays instead of the scattering elastic X-rays. Because the Ti fluorescence X-rays have much lower energies than those of Cu, we could remove them effectively by an Al filter placed before the scintillation counter. The XAFS measurements were carried out at room temperature in the range of 8700−9500 eV. The acquisition time was 10 s for each point, and the measurement for one orientation was repeated seven times.

2.3. XAFS Analysis. The intensity of fluorescence signal normalized with the incidence X-ray flux is expressed as[55]

$$I_f/I_0 = C\frac{\mu(E)}{\mu_{Total}(E) + \mu_{Total}(E_f)\dfrac{\sin\phi}{\sin\theta}} \times \left[1 - \exp\left(-\left(\frac{\mu_{Total}(E)}{\sin\phi} + \frac{\mu_{Total}(E_f)}{\sin\theta}\right)d\right)\right] \quad (2)$$

where C, $\mu_{Total}(E)$, $\mu_{Total}(E_f)$ ϕ, θ, and d are a constant related to detection efficiency, total absorbances at incident X-ray energy and at fluorescence X-ray energy, angles of incident and detection directions with respect to the sample surface, and the sample thickness, respectively. μ is the Cu K edge absorption coefficient. Provided $\sin\phi \approx \phi = 5$ mrad, $d = 3 \times 10^{-8}$ cm, $\mu_{Total}(E) = 4000$ cm^{-1} and $\mu_{Total}(E_f) = 400$ cm^{-1}, eq 2 can approximately be written in the following expression:

$$I_f/I_0(E) \approx C\mu(E)d\sin\theta \quad (3)$$

as

$$\left(\frac{\mu_{Total}(E)}{\sin\phi} + \frac{\mu_{Total}(E_f)}{\sin\theta}\right)d \approx \frac{\mu_{Total}(E)}{\phi}d = 2 \times 10^{-2} \quad (4)$$

Thus, the I_f/I_0 is directly proportional to μ.

In general, XAFS can be partitioned into two parts, i.e., XANES (X-ray absorption near edge structure) in the range of −30 to +50 eV around the edge and EXAFS (extended X-ray absorption fine structure), which appears 50−1000 eV above the edge. XANES reflects the electronic structure and symmetry around an X-ray absorbing atom.[56,57] However, quantitative analysis of XANES is still difficult, and hence, we compared the XANES spectra of the sample with those for reference compounds to characterize the surface state of Cu. XANES data were obtained by the subtraction of preedge background and the normalized by the edge height.

The EXAFS oscillations, $\chi(k)$'s, were extracted by using the program package autobk[58] or Rex2000.[59] The background was estimated by the cubic smoothing method[60] and normalized by the edge height. The origin for the photoelectron kinetic energy was set at the inflection point of the absorption edge. To obtain the rough estimation of coordination numbers, the EXAFS data were first fitted with the following equations with feffit program in an R space or using Rex2000 in a k space[58,59]

$$\mu(k) = \sum_i \frac{S_i N_i F_i(k_i) e^{-2\sigma_i^2 k_i^2}}{k_i r_i^2} \sin(2k_i r_i + \phi_i(k_i))$$

$$k_i = \sqrt{k^2 - 2m_e\ddot{A}E_i/\hbar^2} \quad (5)$$

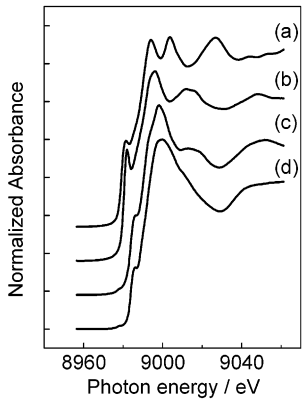

Figure 2. XANES spectra for reference compounds; (a) Cu foil, (b) Cu_2O, (c) CuO, and (d) $Cu(DPM)_2$.

where S_i, N_i, σ_i, and r_i are an inelastic reduction factor, a coordination number, a Debye−Waller factor, and a bond distance for the ith shell. $F_i(k)$ and $\phi_i(k)$ are a backscattering amplitude and a phase shift function for the ith shell, respectively. The backscattering amplitude $F_i(k)$ and phase shift $\phi_i(k)$ were calculated using FEFF8.0.[61] ΔE_i is a difference between experimentally determined photoelectron kinetic energy zero and that used for the theoretical calculation for phase shift and amplitude functions of the ith shell. The inelastic reduction factors, S for Cu−O and Cu−Cu, are estimated by using reference compounds, $Cu(DPM)_2$ and Cu foil, where the coordination numbers were 4 and 12, respectively. The degree of fitting was evaluated with the R factor defined as follows:

$$R = \frac{\sum(k^3\chi_{obs}(k) - k^3\chi_{calc}(k))^2}{\sum(k^3\chi_{obs}(k))^2} \quad (6)$$

In the polarization dependent experiment, we obtained a polarization dependent coordination number, which is called as effective coordination number. The final structure was determined by an iteration method using FEFF8.0 and a real-space model structure.[41,62] In this model, we assumed no significant reconstruction of the TiO_2 surface as an initial guess.

3. Results and Discussion

3.1. XAFS for Reference Cu Compounds. Figure 2 shows XANES spectra of Cu foil, Cu_2O, CuO and $Cu(DPM)_2$. The inflection point appeared at 8979.2, 8980.9, 8983.9, and 8983.9 eV for Cu foil, Cu_2O, CuO and $Cu(DPM)_2$, respectively. This sequence well corresponds to their oxidation states. The inflection point of the XANES spectra for other Cu^{2+} compounds, $Cu(acac)_2$ and $CuSO_4{\cdot}5H_2O$, appeared at 8982 and 8988 eV, respectively. The inflection point for $CuSO_4{\cdot}5H_2O$ is higher than those of the other Cu^{2+} compounds probably because the presence of SO_4^{2-} which plays a strong acidic site and withdraws electrons from Cu. We can safely say that the energy at the inflection point higher than 8982 eV indicates a Cu^{2+} state. Figure 3 shows the $\chi(k)$ and their corresponding Fourier transforms for some reference compounds, Cu_2O, CuO, $Cu(DPM)_2$, $Cu(acac)_2$, and $CuSO_4{\cdot}5H_2O$. To see the validity of the FEFF8-calculated phase shift and amplitude functions, we carried out curve fitting analyses for these reference compounds. Table 1 summarized the curve fitting results. These results well coincide with the bond distances and coordination numbers derived from X-ray crystallography as shown in Table 1.

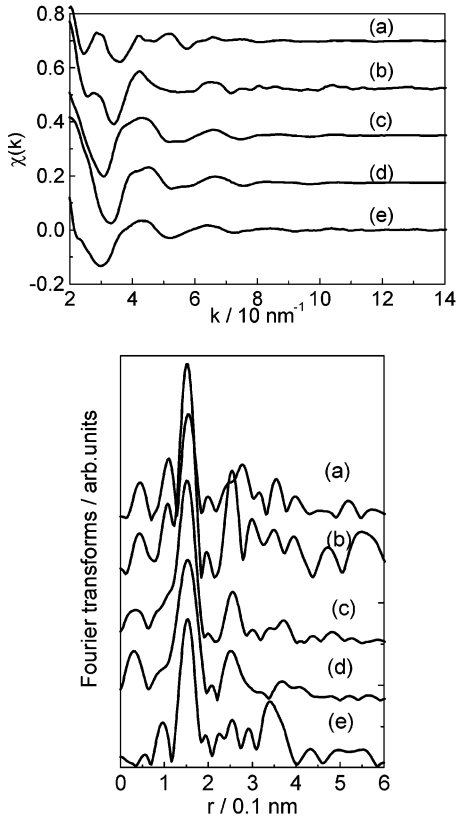

Figure 3. XAFS oscillations and their Fourier transforms for (a) Cu_2O, (b) CuO, (c) $Cu(DPM)_2$, (d) $Cu(acac)_2$, and (e) $Cu(SO_4)\cdot 5H_2O$.

TABLE 1: Curve Fitting Results for Cu Reference Compounds

compound	bond	N [a]	r[a]/nm	$\Delta\sigma^2$/ 10^{-5} nm	ΔE/ eV	ref
Cu_2O	Cu−O	1.5(2)	0.186(0.1848)	0	5	83
CuO	Cu−O	3.6(4)	0.195(0.197)	3	4	84
$Cu(DPM)_2$	Cu−O	(4)	0.191	(0)	4	this work
$Cu(acac)_2$	Cu−O	4.0(4)	0.191(0.191)	0	6	85
$CuSO_4\cdot 5H_2O$	Cu−O	3.7(4)[b]	0.195(0.196)	1	6	86

[a] Crystallographic data are given in the parentheses. [b] $CuSO_4\cdot 5H_2O$ has an octahedral structure but axial Cu−O bonds are elongated to 0.2385 nm, due to Jahn−Teller effect.

3.2. XAFS Spectra for As-Deposited Species. Figure 4 shows the XANES spectra of as-deposited Cu species on a TiO_2(110). A little difference was found in the spectra in the three different orientations. A shoulder structure appeared only in the [001] direction, but it was less clear than that observed in original $Cu(DPM)_2$. The inset in Figure 4 depicted the comparison of XANES spectra between the as-deposited Cu species on TiO_2(110) averaged over three directions and the $Cu(DPM)_2$ powder. If the modification in the $Cu(DPM)_2$ structure after the deposition on the TiO_2 surface was small, both spectra should agree or resemble each other. Thus, the XANES results indicated that the $Cu(DPM)_2$ did not adsorb molecularly on the TiO_2 keeping its original structure. The edge inflection points appeared at 8982, 8984, and 8984 eV for [001], [1$\bar{1}$0], and [110], respectively. Comparison with the reference compounds demonstrates that Cu is in a divalent state. The lower energy of the inflection point for the [001] direction may be due to the small shoulder structure.

Figure 5 shows the *k*-weighted EXAFS oscillations and their Fourier transforms for Cu species on TiO_2(110). A main peak appeared at almost the same position in the three directions, and the peak height in the [110] direction was a little higher than that in the [1$\bar{1}$0] direction, indicating that the Cu atom is located at a rather high symmetric site. Table 2 depicted the curve fitting results of XAFS oscillations for the as-deposited Cu on TiO_2(110) together with other reference compounds and EXAFS data for Cu on inorganic oxides in the literature. The Cu−O bond length was 0.194 nm for all of the directions and the effective coordination numbers were about 4. The distances were in good agreement with those of Cu compounds and $Cu(DPM)_2$ powder in divalent states.

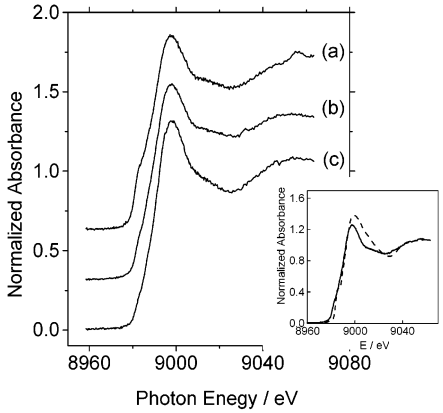

Figure 4. Polarization dependent XANES spectra for the as-deposited Cu/TiO_2(110) (a) *E*||[001], (b) *E*||[1$\bar{1}$0], and (c) *E*||[110]. The data were normalized by the edge height. The inset is a comparison between the averaged XANES spectrum for the polarization dependent XANES of the as-deposited Cu/TiO_2(110) (solid line) and the XANES spectrum for the $Cu(DPM)_2$ (broken line).

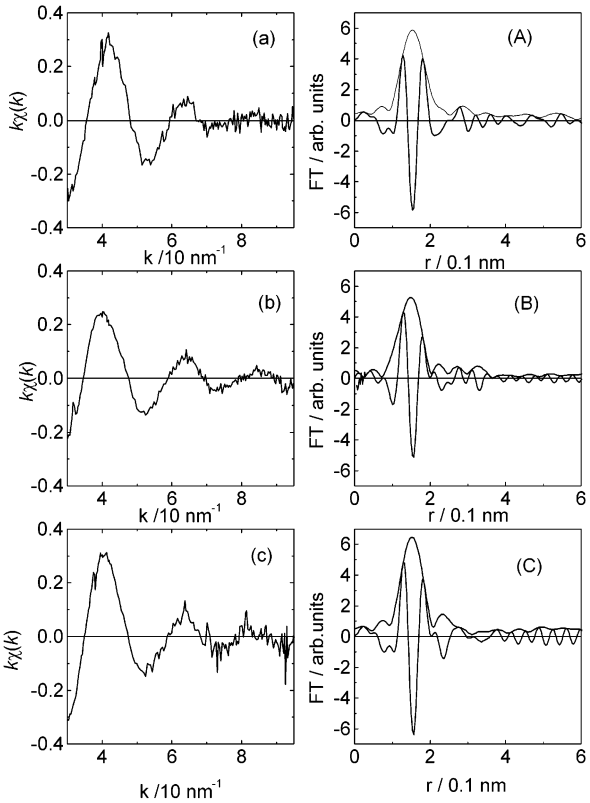

Figure 5. Polarization dependent EXAFS oscillations $k\chi(k)$ (a,b,c) and their Fourier transforms (A,B,C) for the as-deposited Cu/TiO_2(110). Solid and broken lines in the Fourier transforms indicate the absolute and imaginary parts of the Fourier transformations, respectively. (a,A) *E*||[001], (b,B) *E*||[1$\bar{1}$0], and (c,C) *E*||[110].

TABLE 2: Curve Fitting Results for As-Deposited Cu on TiO_2(110) and Other Cu Species

orientation or samples	bond	N^a	r/nm	$\Delta\sigma^2/10^{-5}$ nm^2	ΔE/eV	R/%	ref
[001]	Cu−O	4.0 ± 0.4	0.194 ± 0.002	4 ± 2	4 ± 1	2.9	this work
[1$\bar{1}$0]	Cu−O	4.2 ± 0.4	0.193 ± 0.002	4 ± 2	4 ± 1	3.5	
[110]	Cu−O	3.8 ± 0.4	0.194 ± 0.002	4 ± 2	4 ± 1	2.0	
CuO	Cu−O	4	0.197				84
Cu_2O	Cu−O	2	0.1848				83
$Cu(DPM)_2$	Cu−O	4	0.191				this work
Cu in ZSM-5	Cu−O		0.201				87
Cu in ZSM-5	Cu−O	4	0.195−0.197				88
Cu in ZSM-5	Cu−O	2.8	0.195				89
Cu in Y zeolite	Cu−O	3.6	0.197				90
Cu on α-quartz (0001)	Cu−O	3.2[b]	0.200[b]				91
		3.7[c]	0.202[c]				
Cu on a-quartz (0001)	Cu−O	5.1[b]	0.195[b]				92
		4.3[b]	0.195[b]				
Cu on α-Al_2O_3 (0001)	Cu−O	6.5[b]	0.192[b]				
		5.1[c]	0.193[c]				
Cu on α-Al_2O_3 (1$\bar{1}$02)	Cu−O	6.0[b]	0.193[b]				
		4.4[c]	0.194[c]				

[a] *N* represents effective coordination numbers determined by the polarization dependent experiments. [b] Parallel to the surface. [c] Perpendicular to the surface.

3.3. Structure of As-Deposited Cu Species on TiO_2(110). First, we excluded the possibility of the molecular adsorption of $Cu(DPM)_2$ complex without modification in the structure from the comparison of the XANES spectra for the $Cu(DPM)_2$ powder and the averaged one for the as-deposited Cu sample as shown in Figure 4. The second possibility is $Cu(H_2DPM)_2^{2+}$ that might be formed through the reaction with the surface OH groups of TiO_2(110). Sekine et al. reported $Cu(DPM)_2$ reacted with surface OH groups on SiO_2 and $SrTiO_3$ to produce the ionic species $Cu(H_2DPM)_2^{2+}$ which interacts with surface Si−O$^-$.[49−51] STM revealed that hydrogen atoms are located at the atop site of bridging oxygen atoms of TiO_2(110) to form OH groups.[63] Thus, these hydrogen can react with $Cu(DPM)_2$. The fact that one could find the Cu−O bonds in three directions indicated random orientation of the planar molecule. If this were correct, an isotropic feature should have been observed in XANES. However, the XANES spectrum in the [001] direction only gave the shoulder structure at the edge as shown in Figure 4. Thus, the planar $Cu(H_2DPM)_2^{2+}$ structure cannot explain the isotropic feature in the EXAFS Fourier transforms of Figure 5 and the anisotropic shoulder structures at the edge in the XANES spectra of Figure 4. The appearance of the edge peak only in the [001] direction indicates a preferential alignment of the Cu species at the surface. The shoulder structure at the edge was attributed to the 1s → $4p_\pi^*$ by polarization dependent XANES experiments and ab initio calculations.[64−67] The Cu atom interacts with the conjugated π molecular orbital on DPM to form $4p_\pi^*$. It is suggested that the edge peak structure is most enhanced when the polarization vector and the plane of the DPM ligand is vertical, whereas no shoulder at the edge is observed when the molecular plane is parallel to the polarization vector. Thus, the direction normal to the Cu(DPM) plane should be oriented in the [001] direction. However, in such an orientation of the planar $Cu(DPM)_2$ molecule, no one can find the Cu−O bond in the [001] direction.

A possible structure to satisfy the EXAFS and XANES observations is the Cu(DPM)(O-)$_2$ structure shown in Figure 6. $Cu(DPM)_2$ dissociatively adsorbs on the TiO_2(110) surface, and a DPM ligand is replaced by the oxygen atom(s). Two adsorption sites are possible, i.e., an atop site and a 2-fold site of the bridging oxygen atoms. The adsorption of Cu(DPM) in the troughs as postulated by Newton et al. for the adsorption site of $Rh(CO)_2$[68] could be neglected because the Cu−Ti distance becomes too short when the Cu−O bond is fixed at the bond length of 0.194 nm determined by the TPRF-EXAFS, whereas we could not observe any Cu−Ti interaction in the [110] direction. Because the Cu−O bond should not be observed in the [001] or [1$\bar{1}$0] directions if the Cu (DPM) moiety sits on the atop site of the bridging oxygen, Cu(DPM) should be anchored on the 2-fold site with a tetrahedral coordination, where the direction normal to the Cu(DPM) plane is oriented to the [001] direction as shown in Figure 6. The EXAFS oscillation along the [110] direction was a little larger than that along the [1$\bar{1}$0]. This is probably because the coordination of Cu is not in an ideal tetrahedral structure but elongated to the [110] direction owing to the Jahn−Teller distortion.

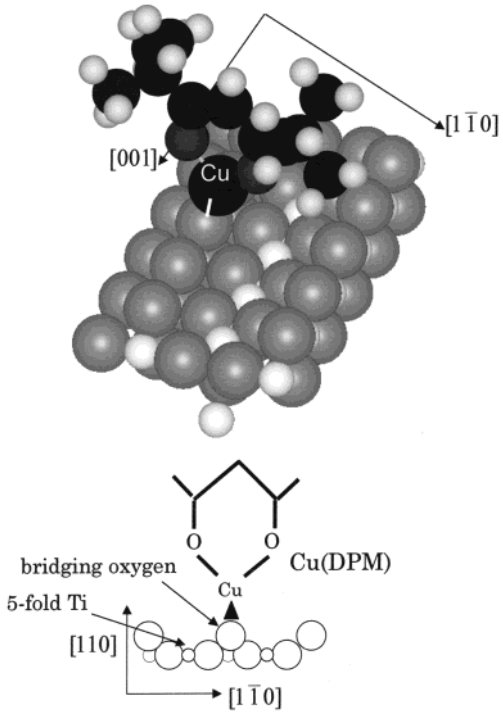

Figure 6. Proposed adsorption structure and site for the as-deposited Cu species on TiO_2(110).

As a consequence, we propose the dissociative adsorption of $Cu(DPM)_2$ to form Cu(DPM) which is attached to the 2-fold site of the bridging oxygen atoms at the TiO_2(110) surface as shown in Figure 6. Hayden et al. claimed that $[Rh(CO)_2Cl]_2$

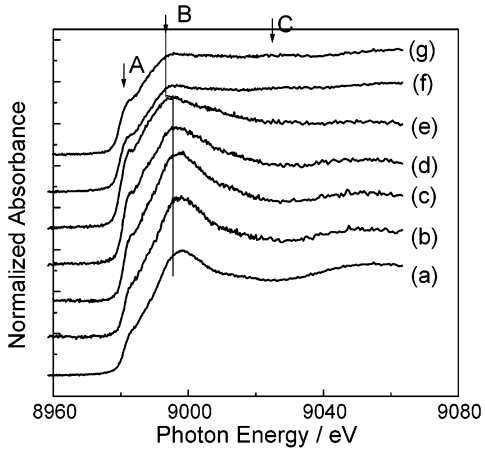

Figure 7. Change of XANES spectra during the H_2 reduction process of the Cu species on TiO_2(110); (a) 313, (b) 323, (c) 333, (d) 343, (e) 353, (f) 363, and (g) 473 K.

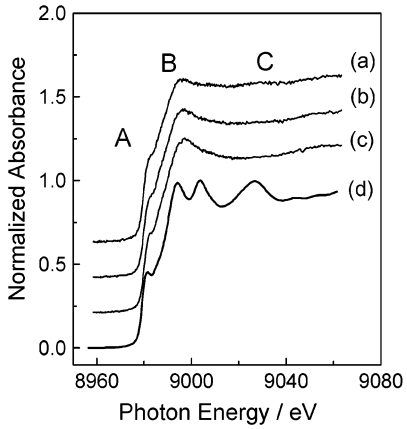

Figure 8. Polarization dependent XANES spectra for the Cu/TiO_2(110) reduced at 363 K in the presence of 1.33 kPa H_2. The data were normalized by the edge height. (a) *E*‖[001], (b) *E*‖[1$\bar{1}$0], and (c) *E*‖[110]. (d) is the XANES spectrum for Cu foil.

adsorbed on the 2-fold site of the bridging oxygen atoms as $Rh(CO)_2$ with a preferential alignment of the Rh−CO along the [1$\bar{1}$0] direction.[68] However, afterward, Evans et al. proposed that $[Rh(CO)_2Cl]_2$ dissociatively adsorbed on TiO_2(110) to form the $[Rh(CO)_2]Cl$ species, where the Rh atom in the $[Rh(CO)_2Cl]$ was bound to the atop site of the bridging oxygen atom.[69,70] At the same time, the Rh−Cl bond was directed to the surface to have a Cl −5-fold Ti interaction to stabilize the $Rh(CO)_2Cl$ planar structure and to hold the preferential orientation on the surface. Anyway, the bridging oxygen atoms are the reactive sites to induce bonding with the metal complexes. This findings agree with the theoretical predictions given in the literature, which claimed that the bridging oxygen atoms are the stable adsorption sites for Ni and Pd.[71,72]

3.4. XANES Change during the Reduction Process. To prepare the small Cu cluster in a controllable manner, we reduced the sample while monitoring its XANES. Figure 7 shows in situ XANES spectra for the Cu species deposited on TiO_2(110) during the reduction process with H_2. The polarization vector of the incident X-ray was oriented along the [001] direction of the TiO_2. The sample was exposed to 1.33 kPa H_2 and heated at a ramping rate of 1 K min^{-1}. When the temperature reached the given values, we started XANES measurements, keeping the temperature. The XANES of the Cu species in the [001] direction gave a shoulder at 8984 eV (denoted as peak A) and a peak at 8997 eV (denoted as peak B). At 333 K, absorbance around 9010 eV in the spectrum began to increase as shown in Figure 7d. At 343 K, the peaks A and B shifted to a lower energy side and peak B decreased. A new peak appeared around 9030 eV, denoted as peak C in Figure 7. The change in the spectra seemed to stop at 363 K. The structure was stable when the sample was treated for 10 min at this temperature. We measured the PTRF-XAFS spectra of the Cu species after the reduction at 363 K.

3.5. Polarization Dependent XAFS after the Reduction at 363 K. Figure 8 shows the polarization dependent Cu K edge XANES spectra in three different directions after the reduction of the sample with H_2 at 363 K. The data were normalized with the edge height. There was also a clear polarization dependence in the spectra. Peak C was smallest in the [110] direction, whereas the absorbance of peak B in the [001] direction was the smallest among the three directions. Peak A appeared in the XANES spectra in all directions. Compared with XANES data for the Cu foil in Figure 8, peaks A and C are characteristic of metallic Cu, indicating the presence of a Cu−Cu direct bond

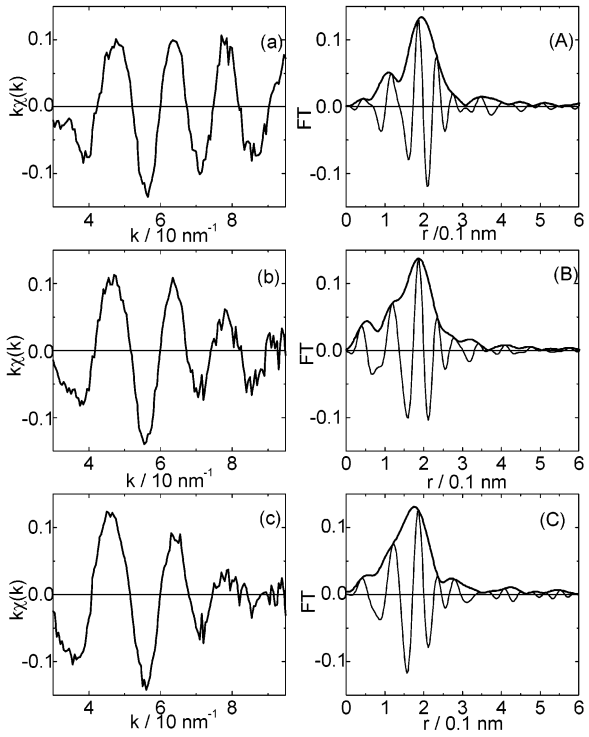

Figure 9. Polarization dependent EXAFS oscillations $k\chi(k)$ (a,b,c) and their Fourier transforms (A,B,C) for the Cu/TiO_2(110) reduced at 363 K in the presence of 1.33 kPa H_2. Solid and broken lines in the Fourier transforms indicate the absolute and imaginary parts of the Fourier transformations, respectively. (a,A) *E*‖[001], (b,B) *E*‖[1$\bar{1}$0], and (c,C) *E*‖[110].

bonding. The inflection points of the edge in the three directions appeared at 8979.5 eV, also suggesting the presence of Cu species in the low-valence state. In Cu foil, peak B is split. According to the multiple scattering calculation, the split of peak B occurs when a Cu atom has coordination shells higher than the third one.[73] A similar ill-structured feature of peak B was observed in small Cu clusters.[74,75] Thus, the XANES data indicate the formation of very small metallic Cu clusters on the TiO_2 surface by reduction at 363 K.

Figure 9 shows the *k*-weighted EXAFS oscillations, $k\chi(k)$ in the three directions and their Fourier transforms. The EXAFS oscillation in the [110] direction damped most quickly than in the other two directions. The peak height of the Fourier transform in the [110] direction is the smallest. In addition, the

TABLE 3: Curve Fitting Results for Cu/TiO_2(110) Reduced at 363 K[a]

orientation	bond	N	r/nm	$\Delta\sigma^2$/10^{-5} nm^2	ΔE/eV	R/%
[001]	Cu−Cu	2.7 ± 0.3	0.244 ± 0.002	0 ± 2	0 ± 5	0.6
[1$\bar{1}$0]	Cu−Cu	2.0 ± 0.5	0.244 ± 0.002	(0)	(0)	5.3
[110]	Cu−Cu	0.9 ± 0.5	(0.244)	(0)	(0)	12

[a] Parentheses indicate the values fixed during the fitting procedure.

peak top position of the absolute part in the Fourier transform in the [110] direction appeared at 0.174 nm, whereas the peak top positions in the [001] and [1$\bar{1}$0] directions are at 0.193 and 0.187 nm, respectively. Note that the Fourier transform peak top position shifted to the shorter side than the real distance owing to phase shift but the relative position should have some meaning. The different bond distances according to the polarization direction indicate that the Cu species should have an anisotropic structure. Then, we carried out the curve fitting analysis to obtain a rough image of the Cu species on the TiO_2(110) surface. We could fit the EXAFS data only by assuming the Cu−Cu bond in the [001] direction as shown in Table 3. The Cu−Cu distance was 0.244 nm, which was by 0.015 nm shorter than that of Cu foil.

For the analysis in the [1$\bar{1}$0] direction, we got a large Debye−Waller factor and a large coordination number in the one-shell fitting. If the EXAFS oscillations in the [1$\bar{1}$0] and [001] directions arose from the same Cu−Cu bond, the Debye−Waller factor should be equal. The faster damping found in the [1$\bar{1}$0] direction might be due to the interference between the EXAFS oscillations of Cu−Cu and Cu-support bonds because the Cu species may have some interaction with the bridging oxygen atoms if it was located in the trough. If one carried out multishell fitting to derive the real structure, one would encounter the correlation problems and could not easily have the definite structure. Instead, we carried out the curve fitting with the Debye−Waller factor fixed to that for the [001] direction to obtain better information about the effective coordination number for the further consideration.

In the [110] direction, we had a very large $\Delta\sigma^2$ and ΔE as a result of the fitting by assuming only the Cu−Cu interaction with 4 adjustable fitting parameters. Because the [110] direction corresponds to the electric vector pointing to the TiO_2 substrate direction, the EXAFS may be most affected by the Cu−substrate interaction. To estimate the Cu−Cu contribution roughly, we fixed r, $\Delta\sigma^2$, and ΔE of Cu−Cu at the values in the [001] direction. The coordination number less than 3 for all of the directions indicates that the Cu cluster formed after the reduction at 363 K has a very small Cu_n ensemble($n < 4$).

3.6. Polarization-Dependent XAFS after the Reduction at 473 K. Figure 10 shows the XANES spectra of the Cu species after the reduction with H_2 (1.33 kPa) at 473 K in the three directions. The spectra became less polarization dependent. The shoulder peak denoted as A appeared for all of the polarization-dependent spectra. Peak B still changed with the polarization. In the [001] direction, peak B was the smallest, whereas it was the strongest in the [110] direction. However, the peak height in the [110] direction decreased compared to that reduced at 363 K.

Figure 11 shows the k-weighted EXAFS oscillations, $k\chi(k)$, and their Fourier transforms in the three directions. Again, the $k\chi(k)$ in the [110] direction damped more quickly than in the other directions. The damping rate decreased compared to the corresponding EXAFS oscillation for the sample reduced at 363 K. The Fourier transform peak appeared at 0.193, 0.192, and

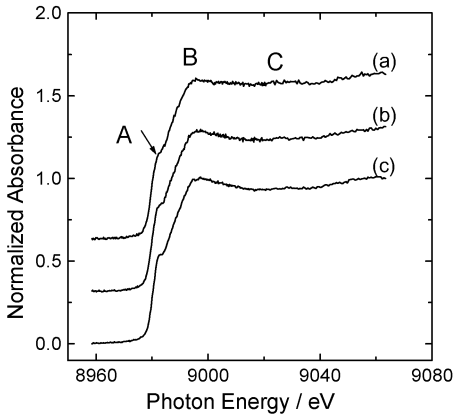

Figure 10. Polarization dependent XANES spectra for the Cu/TiO_2(110) reduced at 473K in the presence of 1.33 kPa H_2. (a) E||[001], (b) E||[1$\bar{1}$0], and (c) E||[110]. The data were normalized by the edge height.

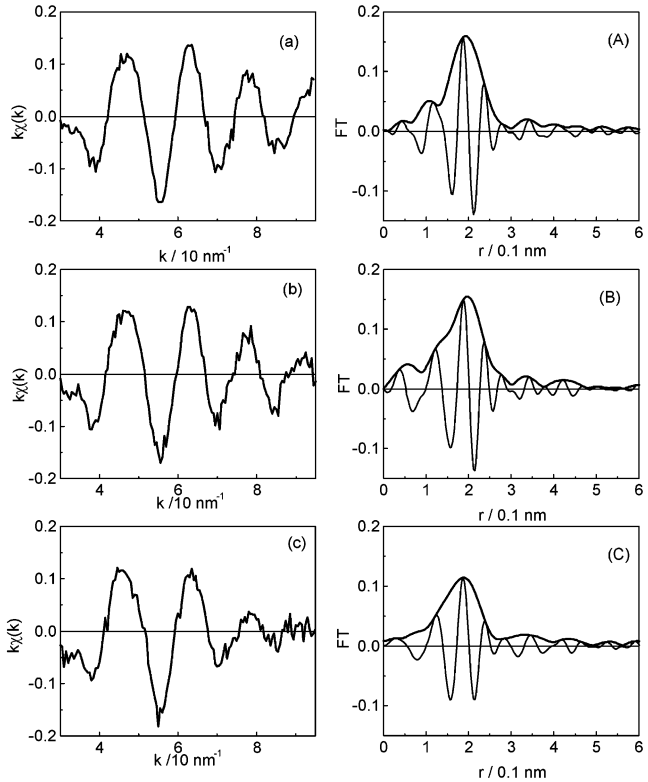

Figure 11. Polarization dependent EXAFS oscillations $k\chi(k)$ (a,b,c) and their Fourier transforms (A,B,C) of the Cu/TiO_2(110) reduced at 473 K in the presence of 1.33 kPa H_2. Solid and broken lines in the Fourier transform indicated the absolute and imaginary parts of the Fourier transformation, respectively. (a,A) E||[001], (b,B) E||[1$\bar{1}$0], and (c,C) E||[110].

TABLE 4: Curve Fitting Results for Cu/TiO_2(110) Reduced at 473 K[a]

orientation	bond	N	r/nm	$\Delta\sigma^2$/10^{-5} nm^2	ΔE/eV	R/%
[001]	Cu−Cu	2.8 ± 0.5	0.245 ± 0.002	0 ± 2	0 ± 5	0.6
[1$\bar{1}$0]	Cu−Cu	2.5 ± 0.5	0.246 ± 0.002	0 ± 2	0 ± 5	1.5
[110]	Cu−Cu	1.7 ± 0.8	0.245 ± 0.002	(0)	(0)	5.3

[a] Parentheses indicate the values fixed during the fitting procedure.

0.187 nm for the polarization vector of E parallel to the [001], [1$\bar{1}$0], and [110] directions, respectively. Table 4 gives the curve fitting results. Cu−Cu bonding at 0.245 nm was found for all of the directions. However, the increase in the coordination number was not so large, indicating that a significant aggregation

did not take place. The ratios of the coordination numbers for the Cu samples treated at 473 K and those at 363 K were 1.0, 1.3, and 1.9 for the [001], [1$\bar{1}$0], and [110] directions, respectively, demonstrating that the cluster growth occurs mainly in the vertical [110] direction after the 473 K reduction.

3.7. Surface Structures of Reduced Cu Species at 363 and 473 K. We first examined the following three possible structures for the Cu_n clusters (n less than 4) on the TiO_2(110) surface produced by the reduction of the as-deposited Cu(DPM) species with H_2 at 363 K. These three structures are based on the model structures previously reported in the literatures.

(a) 3-Dimensional fcc Cluster Growth. The epitaxial fcc Cu metal cluster with its (111) plane parallel to the TiO_2(110) surface has often been reported, where the [1$\bar{2}$1] direction of Cu(110) plane is aligned to the [001] direction of the TiO_2 surface.[16,18,25,28,29,76] Chen et al. reported that 3-dimensional Cu islands grew on TiO_2 at a coverage of 0.03 ML, indicating weak Cu-substrate interaction.[17] Cu is often assumed to be preferably located on the atop line of 5-fold Ti row.[18,29]

(b) 2-Dimensional Cluster or Layer Growth. Ni deposited on TiO_2(110) was claimed to be located in the troughs between the bridging oxygen rows in the one atomic layer structure with the (111) or (100) fcc plane parallel to the TiO_2(110) surface.[77,78]

(c) Linear Species along the [001] Direction. Xu et al. observed Pd dimers with the Pd−Pd bond oriented along the [001] direction by STM.[20] In the Pd dimer, the Pd−Pd distance of 0.298 nm was too long to have a chemical bond.[72] Mo chain structures along the [001] direction of TiO_2(110) were observed in the previous TPRF-XAFS studies where Mo−Mo distance was 0.272 nm. [44]

In the first possibility (a), we should reject a spherical particle growth that would give rather isotropic XAFS spectra because the observed spectra were anisotropic. Even if a hemispherical structure was postulated, we could not reproduce the observed XAFS oscillations, especially in the [110] direction, where a weak Cu−Cu contribution was present in the XAFS. Judging from the weak Cu−Cu contribution in the [110] direction, the height should be less than 2 monolayers. The tetramer model (denoted as Cu_4) obtained by putting a Cu atom on the 3-fold site of a Cu triangle gave a good result for the [001] direction, but the Cu_4 model should have no anisotropy, and it showed a larger oscillations in the [110] direction as shown in Figure 12, where the Cu_4 tetramer was placed at 0.282 nm above the 5-fold Ti site. When the Cu_4 tetramer was located closer to the 5-fold Ti than 0.282 nm, interference between the Ti and Cu XAFS oscillations made the complicated XAFS patterns and we could not get the well- fitted results.

In the second possibility (b), a triangle structure with the plane parallel to the surface could reproduce the XAFS oscillation in the [001] direction but could not reproduce the oscillations in the other two directions as shown in Figure 13. In this model, we assumed the Cu−Ti interaction at 0.244 nm in the [110] direction because we have no Cu−Cu in this direction. This assumption was rationalized by the fact that the difference in the atomic number (Z) of Ti and Cu is so small that the backscattering amplitude and phase shift functions of Ti are not different from those of Cu. The XAFS oscillation in the [1$\bar{1}$0] is a little larger than the observed but the calculation in the [110] direction could not explain the observed XAFS oscillations even if the Cu−Ti(5-fold) bonding was taken into account at 0.244 nm. We simulated the XAFS oscillation by changing the Cu−Ti distance from 0.22 to 27 nm by a 0.01 nm step, but we failed to reproduce the observed data. This is because of the coexistence of Cu−O bonding which interfered

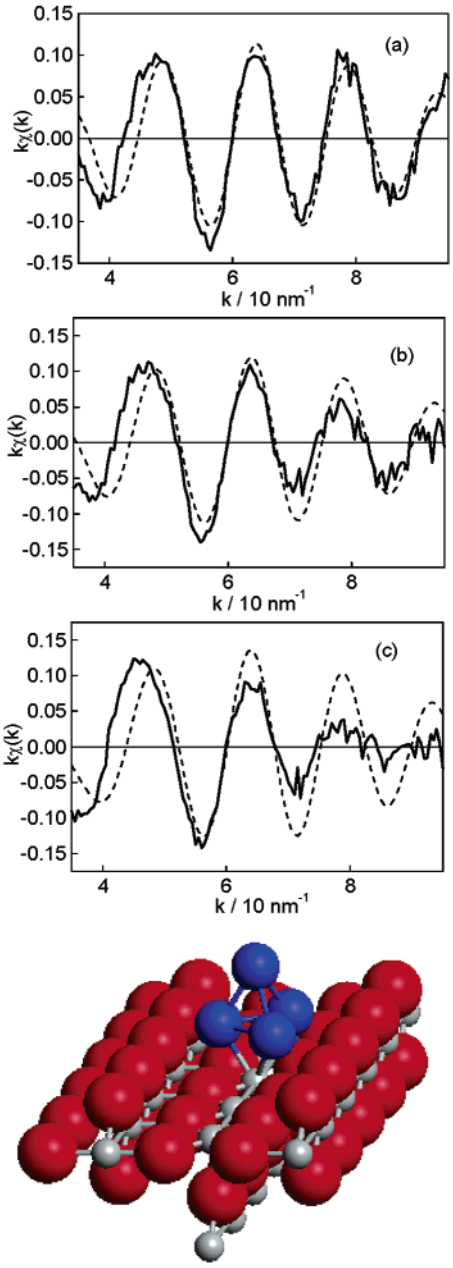

Figure 12. Polarization dependent FEFF simulations for the Cu/TiO_2-(110) after the reduction at 363 K based on a tetramer model as shown in the bottom panel. (a) E||[001], (b) E||[1$\bar{1}$0], and (c) E||[110].

strongly with the Cu−Ti bonding. As a result, the two-dimensional Cu species with the (111) plane model could not reproduce the observed data, either in the [1$\bar{1}$0] or [110] directions. For the same reason, we could not obtain successful results assuming the third possibility (c), linear species along the [001] direction.

The simulations based on the model structures proposed to date never reproduced the observed EXAFS data in the three directions. However, we have learned two facts from the above trials. The agreement between the calculated and observed data in the [001] direction for the tetramer and the planar triangle as shown in Figure 12 and Figure 13 indicated that the effective coordination number in the [001] direction was less than 3 and that contributions from the Cu−substrate bonds were much smaller. The other fact is that we could not reproduce the [110] and [1$\bar{1}$0] by using Cu−Ti and Cu−O bonds without Cu−Cu bonds. Thus, there should be Cu−Cu bonding in both [110]

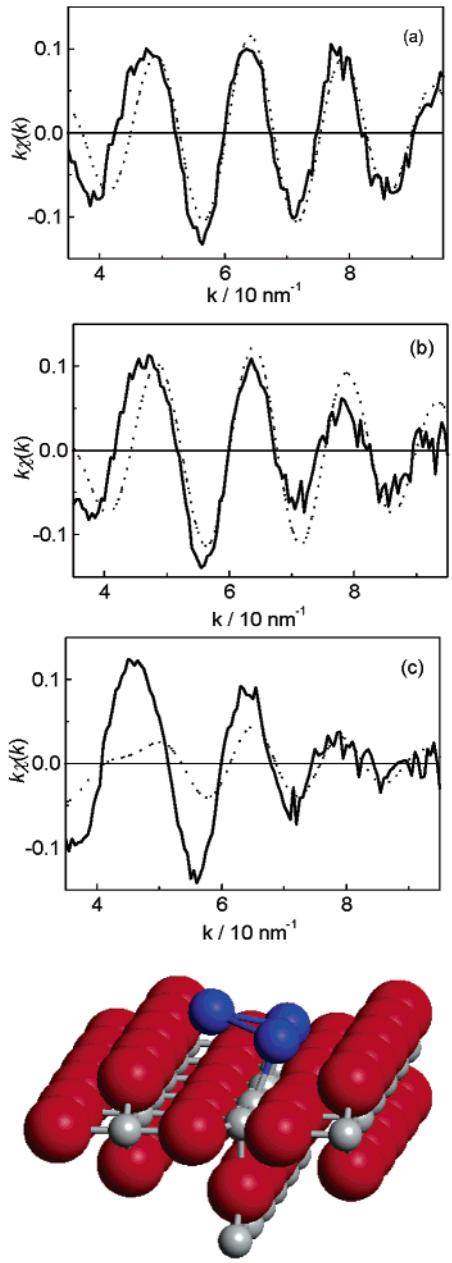

Figure 13. Polarization dependent FEFF simulations for the Cu/TiO_2-(110) after the reduction at 363 K based on a flat triangle model as shown in the bottom panel. (a) *E*||[001], (b) *E*||[1$\bar{1}$0], and (c) *E*||[110]. Solid and broken lines indicate the observed and calculated EXAFS oscillations.

and the [1$\bar{1}$0] directions. However, the coordination number should be much less than 3 because of the failure in the tetramer model.

A model structure we now propose is an inclined trimer model with a Cu−Cu bond distance at 0.244 nm as shown in Figure 14. The inclined angle between the Cu_3 plane and TiO_2(110) surface is about 30°. The inclination of the Cu_3 trimer can reproduce the Cu−Cu oscillation observed in the [110] direction. All Cu atoms are located at atop of the oxygen atoms (2 are on the bridging oxygen atoms and the other is on the in-plane oxygen). The atop site of the bridging oxygen is the one which was theoretically predicted as the favorable adsorption site for metal atoms.[71,72] On the basis of the model shown in Figure 14, we calculated the XAFS oscillations in the three directions. The fitting between the calculated and observed for [110] and [001] are fairly good as shown in Figure 15. Especially in the

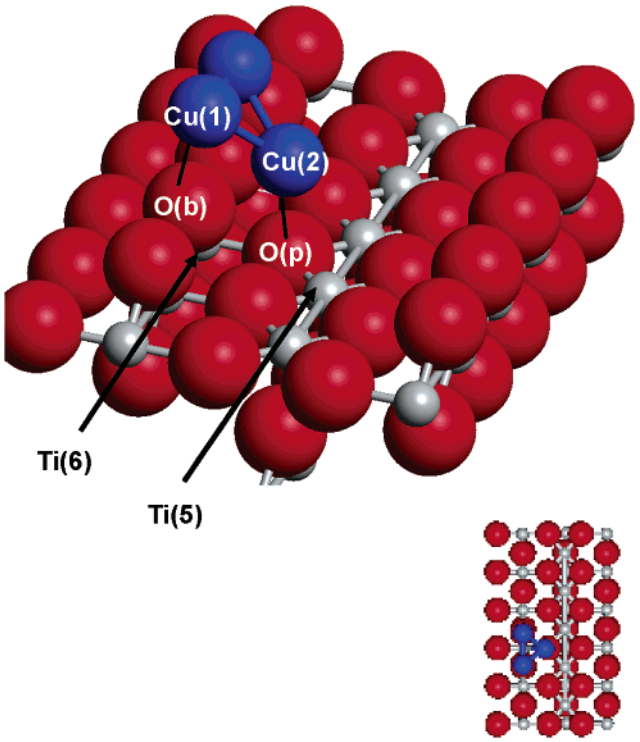

Figure 14. An inclined trimer model for the Cu species on TiO_2(110) after the 363 K reduction.

TABLE 5: List of the Bonds for the Model Structures Shown in Figures 14 and 17[a]

	Figure 14		Figure 17	
bonds	*r*/nm	error/nm	*r*/nm	error/nm
Cu(1)−Cu(2)	0.244	0.002	0.245	0.002
Cu(1)−O(b)	0.233	0.005	0.233	0.01
Cu(2)−O(b)	0.240	0.005		
Cu(2)−O(p)	0.230	0.005	0.230	0.01
Cu(2)−Ti(6)	0.284	0.009		
Cu(2)−Ti(5)	0.31	0.02		

[a] Cu(1), Cu(2), O(b), O(p), Ti(5), and Ti(6) correspond to the ones shown in Figure 14.

[110] direction, it was the first case to succeed in simulating the observed data. However, the oscillation in the [1$\bar{1}$0] direction was not well reproduced in this model structure, which was placed on the nonrelaxed TiO_2 surface.

Charlton et al. claimed that the bridging oxygen atoms moved to a position to have a stronger interaction with deposited Cu atoms.[29] Chun et al. reported a deformation of the bridging oxygen atoms due to the interaction with the Mo dimer.[41,42] We have calculated the EXAFS oscillation based on a locally deformed surface by moving the bridging and in-plane oxygen atoms. The movement was carried out, keeping the local symmetry around Cu. When the antisymmetric movement of bridging oxygen atoms along the [001] direction by 0.015 nm to get closer to Cu with the synchronous upward movement in the [110] directions by 0.01 nm, the calculated XAFS oscillation agreed well with the observed one as shown in Figure 16. Table 5 summarized the bond lengths given in this analysis based on the model structure in Figure 14. The Cu−Cu distance was shorter by 0.015 nm than the bulk value as mentioned above. The Cu−O distances were in the range of 0.230−0.240 nm, which are longer than those observed in Cu oxides (0.195−0.21 nm). Very small metal clusters supported on inorganic oxides are often reported to have longer metal−oxygen bonds than the ones found in metal oxides.[79] Two types of bond lengths

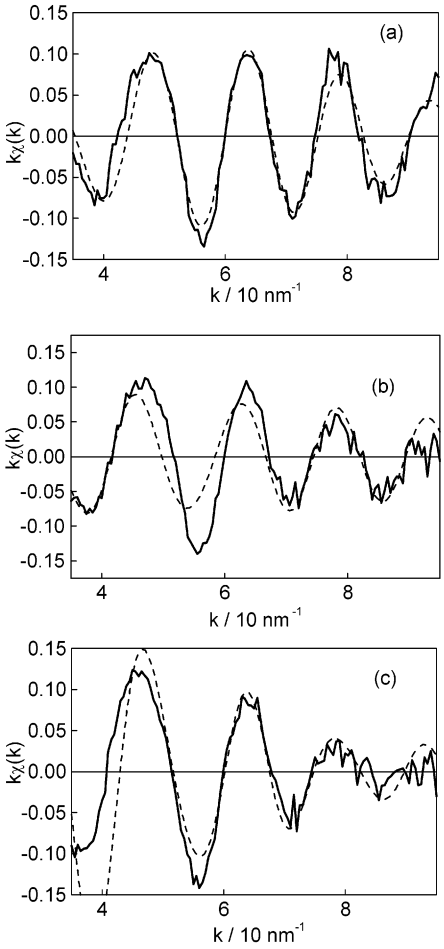

Figure 15. Polarization dependent FEFF simulations for the Cu species on TiO_2(110) shown in Figure 14. The TiO_2(110) surface was assumed to be ideal bulk termination. (a) *E*||[001], (b) *E*||[1$\bar{1}$0], and (c) *E*||[110]. Solid and broken lines indicate the observed and calculated EXAFS oscillations.

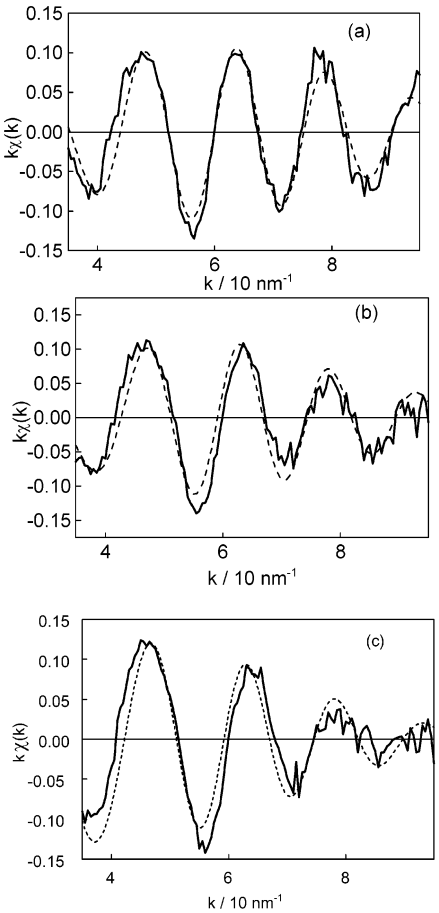

Figure 16. Polarization dependent FEFF simulations for the inclined Cu_3 trimer on a relaxed TiO_2(110) surface after the reduction at 363 K as shown in Figure 14. The modified structure of TiO_2(110) is mentioned in the text. (a) *E*||[001], (b) *E*||[1$\bar{1}$0], and (c) *E*||[110]. Solid and broken lines indicate the observed and calculated EXAFS oscillations.

have been reported in the literature. One is the shorter ones with approximately 0.20−0.24 nm, where the metal clusters have a slightly positive charges due to anchoring to the support oxygen. The other is 0.25−0.28 nm, where there is the van der Waals or hydrogen mediated interaction between O^{2-} and the metallic cluster.[79−81] The presence of hydrogen was postulated at the interface between O^{2-} and the metal clusters because the longer metal−O bonds are often observed after reduction by H_2 at low temperatures without high-temperature postevacuation.[81] The Cu−O bond distances found in this work belong to the former type of bonds. Thus, the interaction of Cu and O is a chemical bond and charge transfer from the Cu to the substrate O occurs. This was supported by the XANES data for the [110] direction. However, the preparation conditions for the Cu cluster corresponds to the conditions of formation of long metal−oxygen bonds because the Cu was reduced at a low temperature, and we measured XAFS of the Cu species under the presence of hydrogen. In our previous work on Pt clusters supported on the α-Al_2O_3(0001) surface, we found the shorter Pt−O bond at 0.22 nm and obtained no evidence for the presence of the longer Pt−O bond.[36] We could not obtain any direct evidence for the presence of long Cu−O distance in this work, either.

The inclined metal clusters have the Cu_3 plane corresponding to the (111) face. Normally in the growth of fcc metals, the (111) plane is parallel to the TiO_2(110) surface.[16,18,25,28,29,76] However, planes other than (111) have also been reported to grow. Onishi et al. reported that the Ni(100) plane was formed in the trough along the [001] direction.[77] Wu et al. reported the inclined (111) plane growth for the Ni overlayer on TiO_2 which corresponds to the (131) plane, where the inclination angle was 27°.[82] It was claimed that the (110) -oriented Cu and Ni planes grew on the TiO_2(110) surface because the lattice matching was most favorable.[10,30] Wagner et al. explained that the discrepancy with the previous results that the fcc metal grew with the (111) face parallel to the TiO_2(110) surface occurred due to the preparation conditions.[30] They prepared Cu films at a high temperature, where the mobility of the Cu atoms was enhanced to form films with less stain. They also postulated that the [1$\bar{1}$0] and [001] directions of the Cu fcc lattice were parallel to the [001] and [1$\bar{1}$0] directions of TiO_2 substrate, respectively. The inclination angle of (111) type facets in the (110) oriented overlayers is 35.3°, which corresponds well to the observed inclination of the Cu_3 triangle in this work. As mentioned above, the inclined Cu_3 (111) plane has strong interactions between the Cu atoms and the bridging and in-plane oxygen atoms as shown in Figure 14.

In our previous work, we proposed a similar inclined Cu_3 structure on TiO_2(110) after the 363 K reduction based on the curve fitting analyses of the polarization dependent EXAFS.[52] There is some discrepancy in the Cu_3 clusters between the previous and present works. The inclining angle of Cu_3 triangles in the previous work was 15°, whereas that in the present work is 30°. The previous model was proposed based on only the coordination numbers derived from the curve fitting analysis,

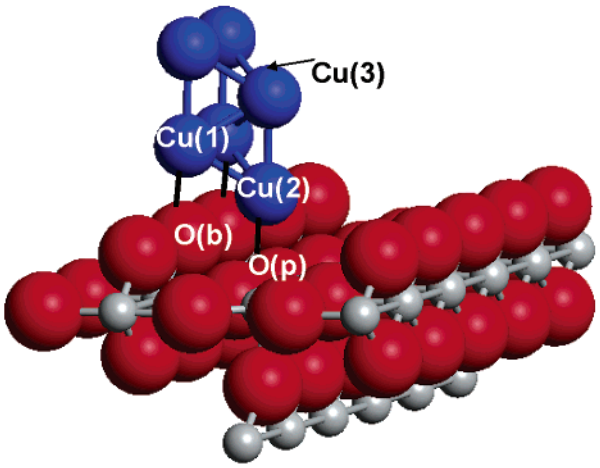

Figure 17. Proposed prismatic model structure for the Cu /TiO_2(110) reduced at 473 K. The second Cu trimer was stacked in the [110] direction.

which gave the smaller coordination number of oxygen than the expected one from the proposed model. Actually, when we applied the iteration method using FEFF8.0 and the real-space model structure, we could not reproduce the EXAFS spectra by the previous Cu_3 model. Thus, the previous model is less plausible. When the Cu_3 species was further reduced at 473 K, we found the vertical growth of the Cu cluster. Provided the growth occurred in the [110] direction of Cu fcc, we put another triangle in the [110] direction of Cu fcc to form the 3 D Cu_6 prismatic cluster as shown in Figure 17. We calculated the EXAFS oscillations on the basis of the prismatic Cu_6 structure and compared them with the observed ones in the three directions. We obtained a good agreement of the calculated and observed data as shown in Figure 18. Thus, the Cu_6 prismatic cluster is the most plausible structure for the Cu species produced by the reduction with H_2 at 473 K. In this structure, the Cu−Cu distance was 0.245 nm, which is shorter than that of Cu foil. We also found the Cu−O bonds around 0.23 nm in the [110] direction. The Cu−Ti contribution became negligibly small.

3.8. Surface Processes to Form Cu Clusters from Cu Organometallic Species on TiO_2(110). The Cu(DPM) species attached to the 2-fold sites of the bridging oxygen atoms on TiO_2(110) were converted to the inclined Cu_3 clusters by reduction at 363 K. During the reduction process, the Cu species and/or Cu atoms can migrate along the [001] direction. To form a triangle structure that has a maximum Cu−Cu interaction, one Cu should move to the 3-fold site in the trough. If the other two Cu atoms are still situated at the 2-fold sites of the bridging oxygen atoms, the shifted Cu atom on the 3-fold site in the trough should have a strong interaction with the 6-fold Ti at a bond length of 0.25 nm. The possibility of such a metal−Ti cation bonding is often mentioned in the literature. Theoretical studies indicate that Pd dimers can interact with 5-fold Ti with Pd−Ti distance at about 0.257 nm[72] though the Pd dimers are not stable. In the present PTRF-XAFS analysis, we could not find Cu−Ti bonding which should strongly modify the XAFS oscillation. Such a short metal−Ti bond may be possible in the alloy where both metals are in metallic states. Cu may be positively charged by the interaction with the electronegative oxygen atoms and repulsive interaction should take place between the Cu cluster and Ti^{4+}. Consequently, the Cu cluster shifts to the other adsorption site where two Cu atoms sit on atop of the bridging oxygen atoms. We found the nearest Cu−Ti bond length to be 0.288 nm, which corresponds to the bond

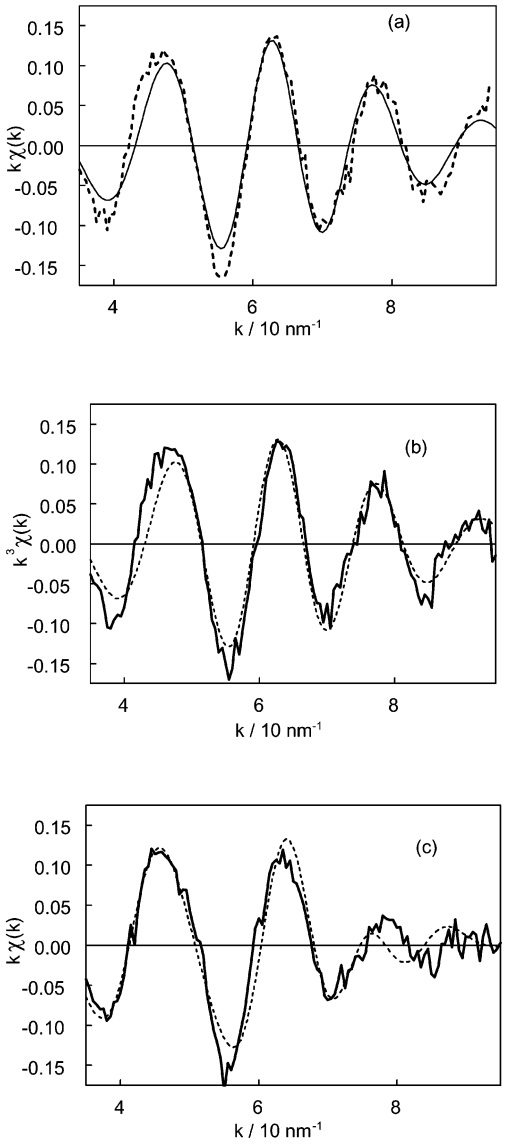

Figure 18. Polarization dependent FEFF simulations for the Cu/TiO_2-(110) after the reduction at 473 K as shown in Figure 17. (a) *E*∥[001], (b) *E*∥[1$\bar{1}$0], and (c) *E*∥[110]. Solid and broken lines indicate the observed and calculated EXAFS oscillations.

length of cation−cation normally found in oxides. Cu_3 clusters were transformed to the Cu_6 prismatic cluster by a vertical growth keeping the Cu_3 unit at 473 K. Such a self-limiting process in the cluster growth can be explained by lattice mismatching. The Cu−Cu distance of the cluster and the O−O distance in the bridging oxygen rows of the ideal bulk structure are 0.244 and 0.296 nm, respectively. Thus, it is difficult to place 3 Cu atoms on the atop sites of the three bridging oxygen atoms. The strong Cu−O at 0.233 nm may hinder the lateral growth of Cu atoms. Furthermore the presence of carbon impurity may prevent the Cu metals from growing.[69] Furthermore, the presence of carbon impurity might prevent the Cu metals from growing.[69] Actually, we found C atoms after the reduction processes by XPS.

3.9. Cu_3 Cluster-Induced Surface Reconstruction of TiO_2-(110). The structure of a clean TiO_2(110) surface has been demonstrated to be relaxed showing downward movement of the bridging oxygen atoms by 0.027 nm,[9] which agreed with the theoretical prediction.[5,8] However, the recent ICISS study suggested little movement of the bridging oxygen.[15] By deposition of Cu thin film on TiO_2(110), the upward shift of the

bridging oxygen atoms occurred together with the movement of the in-plane oxygen atoms to 5-fold Ti atoms.[29] The upward shift of the bridging oxygen atoms from the ideal $TiO_2(110)$ surface was 0.038 nm, while the in-plane oxygen atoms moved by 0.065 nm. In the present work we did not find such large shifts of the oxygen atoms. The bridging oxygen atoms moved by 0.01 nm in the [110] direction and by 0.015 nm in the [001] direction to get closer to the Cu clusters. We could find little relaxation of the in-plane oxygen. It is open to further investigation why we could not detect large movement of the substrate atoms. Nevertheless the surface movements of oxygen atoms are favorable for the formation of stronger interaction between the Cu atoms and the substrate oxygen atoms.

4. Conclusion

Three-dimensional structures of Cu species prepared by the reaction between $Cu(DPM)_2$ and $TiO_2(110)$ single-crystal surface, followed by reduction with H_2 at 363 and 473 K, were investigated by the PTRF-XAFS technique. $Cu(DPM)_2$ dissociatively adsorbed on the 2-fold site of the bridging oxygen atoms with keeping one DPM moiety ($Cu(DPM)(O\text{-})_2$ species). Reduction of the $Cu(DPM)(O\text{-})_2$ at 363 K produced the Cu_3 triangle clusters which leaned against the bridging oxygen rows at about 30° from the $TiO_2(110)$ normal. The Cu−Cu distance was 0.244 nm, and the Cu−O(substrate) distance was 0.23 nm, whereas we could not obtain evidence for direct Cu−Ti bonding. The small Cu_3 cluster was stabilized by the strong interaction between the Cu atoms and the bridging oxygen atoms which provided the anisotropic orientation. Further reduction at 473 K produced the prismatic Cu_6 clusters by stacking the Cu_3 triangle structure in the vertical direction. The Cu−Cu and Cu−O distances were still 0.245 and 0.23 nm, respectively. The triangle cluster behaved as a building unit for metal−metal bonding/cluster growth on $TiO_2(110)$.

Acknowledgment. This study was supported by a Grant-in-Aid for the 21st century COE program for Frontiers in Fundamental Chemistry from the Ministry of Education, Culture, Sports, Science and Technology. The work was also financially supported by CREST programs of JST and a Grant-in-Aid for Scientific Research B(07649766). The XAFS measurements were carried out under the approval of Photon Factory Program Advisory Committee (Proposal No. 98G305, 2000G276, 2002G270).

References and Notes

(1) Henrich, V. E.; Cox, P. A. *The Surface Science and Metal Oxides*; Cambridge University Press: Cambridge, U.K., 1994.
(2) Freund, H.-J. *Surf. Sci.* **2002**, *500*, 271.
(3) Chusuei, C. C.; Lai, X.; Luo, K.; Goodman, W. *Topics Catal.* **2001**, *14*, 1.
(4) Maschhoff, B. L.; Pan, J. M.; Madey, T. E. *Surf. Sci.* **1991**, *259*, 190.
(5) Ramamoorthy, M.; Vanderbilt, D.; King-Smith, R. D. *Phys. Rev. B* **1994**, *49*, 16721.
(6) Reinhardt, P.; Hess, B. A. *Phys. Rev.* **1994**, *50*, 12015.
(7) Vogtenhuber, D.; Podloucky, R.; Neckel, A.; Steinemann, S. G.; Freeman, A. J. *Phys. Rev. B* **1994**, *49*, 2099.
(8) Bates, S. P.; Kresse, G.; Gillan, M. J. *Surf. Sci.* **1997**, *385*, 386.
(9) Charlton, G.; Howes, P. B.; Nicklin, C. L.; Steadman, P.; Taylor, J. S. G.; Muryn, C. A.; Harte, S. P.; Mercer, J.; McGrath, R.; Norman, D.; Turner, T. S.; Thornton, G. *Phys. Rev. Lett.* **1997**, *78*, 495.
(10) Tanner, R. E.; Castell, M. R.; Briggs, G. A. D. *Surf. Sci.* **1998**, *412/413*, 672.
(11) Onishi, H.; Iwasawa, Y. *Surf. Sci. Lett.* **1994**, *313*, L783.
(12) Onishi, H.; Fukui, K.; Iwasawa, Y. *Bull. Chem. Soc. Jpn.* **1995**, *68*, 2447.
(13) Fukui, K.; Onishi, H.; Iwasawa, Y. *Phys. Rev. Lett.* **1997**, *79*, 4202.
(14) Iwasawa, Y. *Surf. Sci.* **1998**, *402*, 8.
(15) Asari, E.; Suzuki, T.; Kawanowa, H.; Ahn, J.; Hayami, W.; Aizawa, T.; Souda, R. *Phys. Rev. B* **2000**, *61*, 5679.
(16) Diebold, U.; Pan, J. M.; Madey, T. E. *Surf. Sci.* **1995**, *331*, 845.
(17) Chen, D. A.; Bartelt, M. C.; Hwang, R. Q.; McCarty, K. F. *Surf. Sci.* **2000**, *450*, 78.
(18) Møller, P. J.; Wu, M. C. *Surf. Sci.* **1989**, *224*, 265.
(19) Schierbaum, K. D.; Fischer, S.; Wincott, P.; Hardman, P.; Dhanak, V.; Jones, G.; Thornton, G. *Surf. Sci.* **1997**, *391*, 196.
(20) Xu, C.; Lai, X.; Zajac, G. W.; Goodman, D. W. *Phys. Rev. B* **1997**, *56*, 13464.
(21) Mostefa-Sba, H.; Domenichini, B.; Bourgeois, S. *Surf. Sci.* **1999**, *437*, 107.
(22) Su, C.; Yeh, J. C.; Lin, J. L.; Lin, J. C. *Appl. Surf. Sci.* **2001**, *169*, 366.
(23) Tamura, K.; Kudo, M.; Owari, M.; Nihei, Y. *Chem. Lett.* **1986**, 1921.
(24) Tamura, K.; Owari, M.; Nihei, Y. *Bull. Chem. Soc. Jpn.* **1988**, *61*, 1539.
(25) Pan, J. M.; Maschhoff, B. L.; Diebold, U.; Madey, T. E. *Surf. Sci.* **1993**, *291*, 381.
(26) Steinruck, H. P.; Pesty, F.; Zhang, L.; Madey, T. E. *Phys. Rev. B* **1995**, *51*, 2427.
(27) Suzuki, T.; Souda, R. *Surf. Sci.* **2000**, *448*, 33.
(28) Diebold, U.; Pan, J. M.; Madey, T. E. *Phys. Rev. B* **1993**, *47*, 3868.
(29) Charlton, G.; Howes, P. B.; Muryn, C. A.; Raza, H.; Jones, N.; Taylor, J. S. G.; Norris, C.; McGrath, R.; Norman, D.; Turner, T. S.; Thornton, G. *Phys. Rev. B* **2000**, *61*, 16117.
(30) Wagner, M.; Kienzel, O.; Bonnell, D. A.; Ruele, M. *J. Vac. Sci. Technol.* **1998**, *16*, 1078.
(31) Tanner, R. E.; Goldfarb, K.; Castell, M.; Briggs, G. A. *Surf. Sci.* **2001**, *486*, 167.
(32) Bart, J. C.; Vlaic, G. *Adv. Catal.* **1987**, *35*, 1.
(33) *X-ray Absorption Fine Structure for Catalysts and Surfaces*; Iwasawa, Y., Ed.; World Scientific: Singapore, 1996.
(34) Shirai, M.; Iwasawa, Y. In *X-ray Absorption Fine Structure for Catalysts and Surfaces*; Iwasawa, Y., Ed.; World Scientific: Singapore, 1996; p 332.
(35) Chun, W. J.; Asakura, K.; Iwasawa, Y. *Appl. Surf. Sci.* **1996**, *100/101*, 143.
(36) Asakura, K.; Chun, W. J.; Shirai, M.; Tomishige, K.; Iwasawa, Y. *J. Phys. Chem.* **1997**, *101*, 5549.
(37) Ijima, K.; Ohminami, Y.; Suzuki, S.; Asakura, K. *Topics Catal.* **2002**, *18*, 125.
(38) Asakura, K.; Chun, W.-J.; Iwasawa, Y. *Topics Catal.* **2000**, *10*, 209.
(39) Parratt, L. G. *Phys. Rev.* **1954**, *95*, 359.
(40) Heald, S. M.; Keller, E.; Stern, E. A. *Phys. Lett.* **1984**, *103A*, 155.
(41) Chun, W. J.; Asakura, K.; Iwasawa, Y. *Chem. Phys. Lett.* **1998**, *288*, 868−872.
(42) Chun, W.-J.; Asakura, K.; Iwasawa, Y. *J. Phys. Chem.* **1998**, *102*, 9006−9014.
(43) Chun, W. J.; Asakura, K.; Iwasawa, Y. *Catal. Today* **1998**, *44*, 309−314.
(44) Chun, W.-J.; Asakura, K.; Iwasawa, Y. *Catal. Today* **2001**, *66*, 97−103.
(45) Iwasawa, Y. *Adv. Catal.* **1987**, *35*, 187.
(46) Iwasawa, Y. *Catal. Today* **1993**, *18*, 21.
(47) *Tailored Metal Catalysts*; Iwasawa, Y., Ed.; D. Reidel: Dordrecht, The Netherlands, 1986.
(48) Iwasawa, Y. *Stud. Surf. Sci. Catal.* **1996**, *101*, 21.
(49) Sekine, R.; Kawai, M.; Asakura, K.; Hikita, T.; Kudo, M. *Surf. Sci.* **1992**, *278*, 175.
(50) Sekine, R.; Kawai, M.; Asakura, K.; Hikita, T.; Kudo, M. *Jpn. J. App. Phys.* **1993**, *32−2*, 431.
(51) Hikita, T.; Sekine, R.; Hanada, T.; Kawai, M. *Surf. Sci. Lett.* **1992**, *262*, L139.
(52) Tanizawa, Y.; Chun, W. J.; Shido, T.; Asakura, K.; Iwasawa, Y. *J. Synchrotron Rad.* **2001**, *8*, 508.
(53) Chun, W. J.; Tanizawa, Y.; Shido, T.; Iwasawa, Y.; Nomura, M.; Asakura, K. *J. Synchrotron Rad.* **2001**, *8*, 168.
(54) Nomura, M.; Koyama, A. *KEK−Rep.* **1996**, 95-15, KEK.
(55) Troeger, L.; Arvanitis, D.; Baberschke, K. *Phys. Rev. B* **1992**, *46*, 3283.
(56) Kosugi, N. In *X-ray Absorption Fine Structure for Catalysis and Surfaces*; Iwasawa, Y., Ed.; World Scientific: Singapore, 1996; p 60.
(57) Fujikawa, T. In *X-ray Absorption Fine Structure for Catalysis and Surfaces*; Iwasawa, Y., Ed.; World Scientific: Singapore, 1996; p 76.
(58) Stern, E. A.; Newville, M.; Ravel, B.; Yacoby, Y.; Haskel, D. *Physica B* **1995**, *208*, 117.
(59) Asakura, K. In *X-ray Absorption Fine Structure for Catalysts and Surfaces*; Iwasawa, Y., Ed.; World Scientific: Singapore, 1996; p 33.
(60) Cook, J. W.; Sayers, D. E. *J. Appl. Phys.* **1981**, *52*, 5024.

(61) Ankudinov, A. L.; Ravel. B.; Rehr, J. J.; Conradson, S. D. *Phys. Rev. B* **1998**, *58*, 7565.
(62) Chun, W.-J.; Ph.D. Thesis, The University of Tokyo, Tokyo, Japan, 1997.
(63) Suzuki, S.; Fukui, K.; Onishi, H.; Iwasawa, Y. *Phys. Rev. Lett.* **2000**, *84*, 2156.
(64) Kosugi, N.; Yokoyama, T.; Asakura, K.; Kuroda, H. *Chem. Phys.* **1984**, *91*, 249.
(65) Kosugi, N.; Yokoyama, T.; Kuroda, H. *Chem. Phys.* **1986**, *104*, 449.
(66) Kosugi, N.; Yokoyama, T.; Kuroda, H. *Chem. Phys.* **1986**, *103*, 101.
(67) Kosugi, N. In *Core Level Spectroscopy in Condensed Systems*; Kotani, A., Ed.; Springer: Berlin, 1988; p 203.
(68) Hayden, B. E.; King, A.; Newton, M. A. *Chem. Phys. Lett.* **1997**, *269*, 485.
(69) Evans, J.; Hayden, B. E.; Newton, M. *Surf. Sci.* **2000**, *462*, 169.
(70) Bennett, R. A.; Newton, M. A.; Smith, R. D.; Bowker, M.; Evans, J. *Surf. Sci.* **2001**, *487*, 223.
(71) Cao, P. L.; Ellis, D. E.; Dravid, V. P. *J. Mater. Res.* **1999**, *14*, 3684.
(72) Bredow, T.; Pacchioni, G. *Surf. Sci.* **1999**, *426*, 106.
(73) Greaves, G. M.; Durham, P. J.; Diakun, G.; Quinn, P. *Nature* **1981**, *294*, 139.
(74) Montano, P. A.; Shenoy, G. K.; Alp, E. E.; Schulze, W.; Urban, J. *Phys. Rev. Lett.* **1986**, *56*, 2076.
(75) Gota, S.; Gautier, M.; Douillard, L.; Thromat, N.; Duraud, J. P.; Le Fevre, P. *Surf. Sci.* **1995**, *323*, 163.
(76) Wagner, T.; Marien, J.; Duscher, G. *Thin Solid Films* **2001**, *398*, 419.
(77) Onishi, H.; Aruga, T.; Egawa, C.; Iwasawa, Y. *Surf. Sci.* **1990**, *233*, 261.
(78) Bourgeois, S.; Le Seigneur, P.; Perdereau, M.; Chandesris, D.; L Fevre, P.; Magnan, H. *Thin Solid Films* **1997**, *304*, 267.
(79) Koningsberger, D. C.; Gates, B. C. *Catal. Lett.* **1992**, *14*, 271−277.
(80) van Zon, J. B. A. D.; Koningsberger, D. C.; van't Blik, H. F. J.; Prins, R.; Sayers, D. E. *J. Chem. Phys.* **1984**, *80*, 3914.
(81) Koningsberger, D. C.; van Zon, F. B. M.; Vaarkamp, M.; Munoz-Paez, A. In *X-ray Absorption Fine Struture for Catalysts and Surfaces*; Iwasawa, Y., Ed.; World Scientific: Singapore, 1996; p 257.
(82) Wu, M. C.; Moller, P. J. *Surf. Sci.* **1992**, *279*, 23.
(83) Restori, R.; Schwarzenbach, D. *Acta Crystallogr.* **1986**, *42*, 201.
(84) Asbrink, S.; Waskowska, A. *J. Phys., Cond. Matter* **1991**, *3*, 8173.
(85) Shimata, S.; Sasase, T.; Ohta, M. *J. Mol. Struct.* **1983**, *96*, 347.
(86) Bacon, G. E.; Titterton, D. H. *Z. Kristallogr.* **1975**, *141*, 330.
(87) Hamada, H.; Matsubayashi, N.; Shimada, H.; Kintaichi, Y.; Ito, T.; Nishijima, A. *Catal. Lett.* **1990**, *5*, 189.
(88) Grunert, W.; Hayes, N. W.; Joyner, R. W.; Shpiro, E. F.; Siddiqui, M. R. H.; Baeva, G. N. *J. Phys. Chem.* **1994**, *98*, 10832.
(89) Yamaguchi, A.; Shido, T.; Inada, Y.; Kogure, T.; Asakura, K.; Nomura, M.; Iwasawa, Y. *Bull. Chem. Soc. Jpn.* **2001**, *74*, 801.
(90) Tanabe, S.; Matsumoto, H. *Chem. Lett.* **1989**, 539.
(91) Shirai, M.; Asakura, K.; Iwasawa, Y. *Chem. Lett.* **1992**, 1037.
(92) Fitts, J. P.; Trainor, T. P.; Grolimund, D.; Bargar, J. R.; Parks, G. A.; Brown, G. E. *J. Synchrotron Rad.* **1999**, *6*, 627−629.